FRONTIERS OF PHYSICS

RESEARCH ARTICLE
Volume 21 / Issue 12 / 124203 / 2026

Transfer matrix method for periodic space-time modulated system

Xiaohui Zhu[1,†], Chen Shen[2]

1 Huzhou Key Laboratory of Green Energy Materials and Battery Cascade Utilization, School of Intelligent Manufacturing, Huzhou College, Huzhou 313000, China
2 Department of Mechanical Engineering, Rowan University, Glassboro, New Jersey 08028, USA
Corresponding author. E-mail: †zhuxiaohui@zjhzu.edu.cn
Received September 12, 2025; accepted March 30, 2026

© Higher Education Press 2026

ABSTRACT

Space-time modulation provides a powerful approach for controlling wave behavior and enables forms of wave manipulation that are unattainable in stationary systems. Here, we propose a generalized transfer matrix method for analyzing wave propagation in periodic space-time modulated systems. The proposed method relaxes the commonly assumed sinusoidal modulation constraint and accommodates an arbitrary number of time-varying components with general periodic modulations. A two-membrane acoustic system subjected to three representative periodic modulations — namely, square-wave modulation, triangular-wave modulation, and sawtooth-wave modulation — is investigated. The results demonstrate that the proposed method enables accurate and efficient analysis of weakly modulated space-time periodic systems. This framework provides a versatile tool for analyzing complex space-time modulated structures and may facilitate the development of advanced acoustic devices for applications such as underwater communication, medical ultrasound, and noise control.

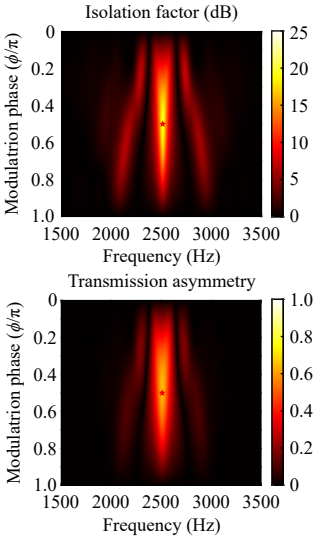

Keywords acoustic metamaterial, space-time modulation

1 Introduction

Recently, wave propagation in space-time modulated systems has attracted considerable attention. A new class of metamaterials whose constitutive parameters vary in both space and time has been proposed and extensively studied in electromagnetics [1–10], acoustics [11–25] and mechanics [26–29]. By introducing time as an additional design degree of freedom, these space-time modulated metamaterials offer unprecedented opportunities for wave manipulation. Various functional devices have been realized based on space-time modulation, including circulators [1, 11, 12, 28], isolators [13, 16–18], amplifiers [3, 5, 6, 19, 23] and metasurfaces [2, 8–10, 20–22]. Recently, increasing attention has been devoted to temporal interfaces. Wave scattering at temporal interfaces can be regarded as the time-domain counterpart of that at spatial interfaces, giving rise to so-called temporal reflection and refraction [30–32]. Unlike spatial interfaces [33, 34], temporal interfaces do not conserve energy, thereby enabling the possibility of broadband amplification [35]. Furthermore, temporal interfaces can serve as fundamental building blocks for general time-varying metamaterials and photonic/phononic time crystals, making them even more intriguing [36–38].

*Special Topic: Advances in Metamaterials: From Theory to Applications Enabled by Functional Units (Editor(s): Huanyang Chen, Minghui Lu & Yangyang Fu).

Higher Education Press

https://doi.org/10.15302/frontphys.2026.124203

However, the introduction of time-varying parameters also brings difficulties in system analysis. Theoretical calculation methods for space-time modulated systems remain scarce and are often limited to simple modulation profiles such as sinusoidal modulation. The most primitive and direct method is to solve the coupled differential equations of the wave envelope, which is originally commonly used in time-varying transmission lines [39, 40] and recently has been extended to modern space-time modulated systems [14]. In this method, only the incident mode and the first-order generated mode are taken into consideration, and all other possible higher-order generated modes are neglected, which may lead to significant inaccuracies [15, 25]. Space-time Floquet theory [26, 41], on the other hand, focuses on mode coupling and predicts all possible coupled modes in the space-time modulated systems. However, it mainly provides a qualitative description and cannot predict the detailed wave evolution during propagation. Furthermore, the theoretical models of the above two methods assume infinitely long, continuous media, which is somewhat inconsistent with realistic implementations.

To solve the above challenges, we propose a transfer matrix method in our previous work [15], which facilitates the investigation of high-order modes generation during propagation and enables the analysis of finite, discretized space-time modulated systems. This method provides a fast yet reliable approach to predict various acoustic effects and functionalities in one-dimensional space-time modulated metamaterials [15, 19, 25]. Nevertheless, this transfer matrix method still faces certain drawbacks when dealing with specific space-time systems. For example, like many other approaches, this method is only applicable to sinusoidal modulation, which is the simplest modulation profile in physics and mathematics. However, when it comes to experimental implementation, sinusoidal modulation poses significant challenges, especially when multiple elements need to be modulated simultaneously with different modulation parameters. In fact, considering experimental feasibility, researchers have adopted a more conservative strategy in the study of space-time modulated metamaterials. Binary temporal modulation (on/off), the simplest modulation profile in practice, is highly favored in the design of space-time modulated metamaterials and can produce versatile effects [20, 42]. Based on the above considerations, we extend our transfer matrix method. Periodic space-time modulation represents a promising direction for advancement. On the one hand, some forms of periodic temporal modulation is relatively easy to implement in practice. The binary modulation mentioned above is a typical example of periodic modulation and has already been successfully demonstrated. On the other hand, there exists a well-established mathematical tool to connect periodic space-time modulation with sinusoidal modulation: Fourier expansion. Based on Fourier expansion, any periodic modulation can be decomposed into multiple sinusoidal components with different modulation frequencies. Grounded in this central idea and substantiated by rigorous mathematical derivations, we formulate the generalized transfer matrix method for periodic space-time modulated systems in this work.

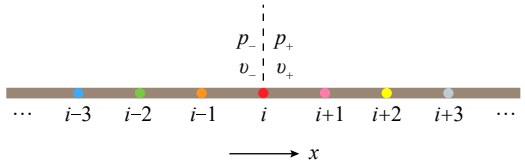

Fig. 1 A 1D acoustic waveguide with periodic time-varying loads. The brown line represents the waveguide. The colored dots denote the periodic time-varying loads.

This paper is organized as follows. First, we establish the model of a one-dimensional acoustic system with periodic space-time modulation and derive its transfer matrix representation. In the derivation, we use an acoustic formulation, but this general formulation can be easily applied to electromagnetic (EM) waves and integrated circuits (ICs). Then, to verify the effectiveness and accuracy of the proposed method, we present the design of an acoustic isolator via a two-membrane system. Three typical periodic modulation profiles, namely square-wave, triangular-wave and sawtooth-wave modulations, are applied to the system. Finally, we discuss the advantages and potential improvements of this generalized transfer matrix method, as well as its limitations and directions for future research.

2 Modeling and matrix representation of a periodic space-time modulated system

Consider a space-time modulated system as shown in Fig. 1, which consists of a one-dimensional waveguide and a series of time-varying loads. Using acoustic waves as an example, we outline the derivation of a series load using the expression for acoustic impedance. For a parallel load, the impedance can be replaced by admittance. Moreover, this general procedure can be readily applied to the study of EM waves and ICs, where one just needs to substitute acoustic pressure and particle velocity (p, v) with electric and magnetic fields (E, H) or voltage and current (U, I).

Assume the impedance varies as a general periodic function $Z(\omega, t+T_p) = Z(\omega, t)$, where ω is the frequency of the acoustic wave propagating in the system, and T_p is the modulation period. Upon applying Fourier series expansion, this modulated impedance can be written as

$$Z(\omega,t) = Z_0(\omega)\left[1+\sum_{N=1}^{\infty} A_N \cos\left(N\Omega t-\phi_N\right)\right], \quad (1)$$

where Z_0 is the impedance without modulation, $\Omega = 2\pi/T_p$ is the modulation frequency, N is the order of harmonic modulation, A_N and ϕ_N are the Fourier coefficients, representing the modulation depth and initial phase of each harmonic modulation component, respectively. Under the weak modulation assumption, we have $A_N \ll 1$.

Due to the varying impedance, a series of harmonics ($\omega_n = \omega_0 + n\Omega$) will be generated under a monochromatic incidence (ω_0). Therefore, the acoustic pressure and velocity upstream (p_-,v_-) and downstream (p_+,v_+) of the load can be written as

$$\begin{cases} p_\pm = \sum\limits_{n=-\infty}^{\infty} P_\pm^n \mathrm{e}^{\mathrm{j}\omega_n t} \\ v_\pm = \sum\limits_{n=-\infty}^{\infty} V_\pm^n \mathrm{e}^{\mathrm{j}\omega_n t} \end{cases}, \tag{2}$$

where $P_\pm^n$ and $V_\pm^n$ represent the complex amplitude of the n^{th} harmonic's pressure and velocity. According to the boundary conditions of the series load, the acoustic pressure and velocity should satisfy the continuity and impedance relations

$$\begin{cases} v_- = v_+ \\ p_- - p_+ = Z v_+ \end{cases}. \tag{3}$$

The expressions for the series load in Eq. (1) as well as the pressure and velocity in Eq. (2) are then substituted into the boundary conditions in Eq. (3). Using Euler's formula $\cos(N\Omega t - \phi_N) = \frac{\mathrm{e}^{\mathrm{j}(N\Omega t - \phi_N)} + \mathrm{e}^{-\mathrm{j}(N\Omega t - \phi_N)}}{2}$, the two boundary condition equations can be rewritten in terms of individual harmonic orders:

$$\begin{cases} V_-^n = V_+^n \\ P_-^n - P_+^n = Z_0^n V_+^n + \sum\limits_{N=1}^{\infty} \left(\frac{1}{2} A_N Z_0^{n-N} \mathrm{e}^{-\mathrm{j}\phi_N} V_+^{n-N} \right) \\ \qquad + \sum\limits_{N=1}^{\infty} \left(\frac{1}{2} A_N Z_0^{n+N} \mathrm{e}^{\mathrm{j}\phi_N} V_+^{n+N} \right) \end{cases}, \tag{4}$$

where $Z_0^n = Z_0(\omega_n)$.

The transfer matrix of the load is defined as follows:

$$\begin{pmatrix} \vdots \\ P_-^{n-2} \\ V_-^{n-2} \\ P_-^{n-1} \\ V_-^{n-1} \\ P_-^{n} \\ V_-^{n} \\ P_-^{n+1} \\ V_-^{n+1} \\ P_-^{n+2} \\ V_-^{n+2} \\ \vdots \end{pmatrix} = M_L \begin{pmatrix} \vdots \\ P_+^{n-2} \\ V_+^{n-2} \\ P_+^{n-1} \\ V_+^{n-1} \\ P_+^{n} \\ V_+^{n} \\ P_+^{n+1} \\ V_+^{n+1} \\ P_+^{n+2} \\ V_+^{n+2} \\ \vdots \end{pmatrix}. \tag{5}$$

From the boundary conditions in Eq. (4), the transfer matrix of the load can be obtained as:

$$M_L = \begin{pmatrix} & \vdots & \vdots & \vdots & \vdots & \vdots & \vdots & \vdots & \vdots & \vdots & \vdots & \\ \cdots & 1 & Z_0^{n-2} & 0 & \frac{A_1 Z_0^{n-1}}{2}\mathrm{e}^{\mathrm{j}\phi_1} & 0 & \frac{A_2 Z_0^{n}}{2}\mathrm{e}^{\mathrm{j}\phi_2} & 0 & \frac{A_3 Z_0^{n+1}}{2}\mathrm{e}^{\mathrm{j}\phi_3} & 0 & \frac{A_4 Z_0^{n+2}}{2}\mathrm{e}^{\mathrm{j}\phi_4} & \cdots \\ \cdots & 0 & 1 & 0 & 0 & 0 & 0 & 0 & 0 & 0 & 0 & \cdots \\ \cdots & 0 & \frac{A_1 Z_0^{n-2}}{2}\mathrm{e}^{-\mathrm{j}\phi_1} & 1 & Z_0^{n-1} & 0 & \frac{A_1 Z_0^{n}}{2}\mathrm{e}^{\mathrm{j}\phi_1} & 0 & \frac{A_2 Z_0^{n+1}}{2}\mathrm{e}^{\mathrm{j}\phi_2} & 0 & \frac{A_3 Z_0^{n+2}}{2}\mathrm{e}^{\mathrm{j}\phi_3} & \cdots \\ \cdots & 0 & 0 & 0 & 1 & 0 & 0 & 0 & 0 & 0 & 0 & \cdots \\ \cdots & 0 & \frac{A_2 Z_0^{n-2}}{2}\mathrm{e}^{-\mathrm{j}\phi_2} & 0 & \frac{A_1 Z_0^{n-1}}{2}\mathrm{e}^{-\mathrm{j}\phi_1} & 1 & Z_0^{n} & 0 & \frac{A_1 Z_0^{n+1}}{2}\mathrm{e}^{\mathrm{j}\phi_1} & 0 & \frac{A_2 Z_0^{n+2}}{2}\mathrm{e}^{\mathrm{j}\phi_2} & \cdots \\ \cdots & 0 & 0 & 0 & 0 & 0 & 1 & 0 & 0 & 0 & 0 & \cdots \\ \cdots & 0 & \frac{A_3 Z_0^{n-2}}{2}\mathrm{e}^{-\mathrm{j}\phi_3} & 0 & \frac{A_2 Z_0^{n-1}}{2}\mathrm{e}^{-\mathrm{j}\phi_2} & 0 & \frac{A_1 Z_0^{n}}{2}\mathrm{e}^{-\mathrm{j}\phi_1} & 1 & Z_0^{n+1} & 0 & \frac{A_1 Z_0^{n+2}}{2}\mathrm{e}^{\mathrm{j}\phi_1} & \cdots \\ \cdots & 0 & 0 & 0 & 0 & 0 & 0 & 0 & 1 & 0 & 0 & \cdots \\ \cdots & 0 & \frac{A_4 Z_0^{n-2}}{2}\mathrm{e}^{-\mathrm{j}\phi_4} & 0 & \frac{A_3 Z_0^{n-1}}{2}\mathrm{e}^{-\mathrm{j}\phi_3} & 0 & \frac{A_2 Z_0^{n}}{2}\mathrm{e}^{-\mathrm{j}\phi_2} & 0 & \frac{A_1 Z_0^{n+1}}{2}\mathrm{e}^{-\mathrm{j}\phi_1} & 1 & Z_0^{n+2} & \cdots \\ \cdots & 0 & 0 & 0 & 0 & 0 & 0 & 0 & 0 & 1 & 0 & \cdots \\ & \vdots & \vdots & \vdots & \vdots & \vdots & \vdots & \vdots & \vdots & \vdots & \vdots & \end{pmatrix}. \tag{6}$$

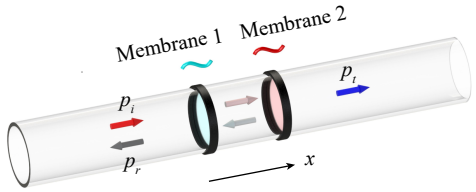

Fig. 2 Schematic of a two-membrane system with modulation. p_i: incident wave. p_r: reflected wave. p_t: transmitted wave.

On the other hand, the transfer matrix of the waveguide can be expressed as follows:

$$M_w = \begin{pmatrix} & \vdots & \vdots & \vdots & \\ \cdots & M_w^{n-1} & 0 & 0 & \cdots \\ \cdots & 0 & M_w^{n} & 0 & \cdots \\ \cdots & 0 & 0 & M_w^{n+1} & \cdots \\ & \vdots & \vdots & \vdots & \end{pmatrix}, \tag{7}$$

where

$$M_w^i = \begin{pmatrix} \cos(k_i l) & jz_0 \sin(k_i l) \\ \dfrac{j}{z_0} \sin(k_i l) & \cos(k_i l) \end{pmatrix}. \tag{8}$$

Here $z_0 = \rho_0 c_0$ is the characteristic impedance of the background medium, $i(= \cdots, n-1, n, n+1, \cdots)$ is the order of harmonics, $k_i = \omega_i / c_0$ is the wave number of the i^{th} harmonics, and l is the length of the waveguide.

For a system composed of Q equally spaced time-varying series loads, the total transfer matrix can therefore be obtained as $M = M_w M_{L_1} M_w M_{L_2} M_w \cdots M_w M_{L_{Q-1}} M_w M_{L_Q} M_w$ by concatenating the individual transfer matrices of the loads and the waveguide. The acoustic response of this periodic space-time modulated system can then be analyzed using the transfer matrix method.

3 Analysis of typical periodic modulations in a space-time modulated membrane system

In this section, we start with a simple acoustic system consisting of a circular tube and two edge-clamped membranes under space-time modulation as shown in Fig. 2. It is assumed that the membranes with modulated tension do not radiate acoustic waves. The parameters are as follows: the radius of the tube and membrane $R = 7.5$ mm, the distance between the two membranes $D = 20$ mm; the density of the background medium $\rho_{air} = 1.21$ kg/m^3 and the sound speed $c_{air} = 343$ m/s; the membrane thickness $d = 0.2$ mm, density $\rho_m = 1300$ kg/m^3, Young's modulus $E_m = 117.5$ kPa and shear modulus $G_m = 40$ kPa. The tube wall is assumed to be acoustically rigid.

The membrane is a typical series load element, and its impedance can be written as

$$Z_m(\omega) = -\mathrm{j}\omega\rho_m d J_0\left(\frac{\omega R}{c_m}\right) / J_2\left(\frac{\omega R}{c_m}\right), \tag{9}$$

where J_0 and J_2 are the 0$^{\text{th}}$ order and 2$^{\text{nd}}$ order Bessel functions of the first kind. Time-varying surface tensions in the form of $T = T_0[1 + mF(t)]^2$ are applied to these two membranes, where m and $F(t)$ are the modulation depth and modulation waveform function, respectively. The surface tension function here needs to be squared to achieve the desired modulated sound speed and impedance, as indicated by the relation $c_m = \sqrt{\frac{T}{\rho_m d}}$. Under the weak modulation ($m \ll 1$), we can expand the impedance at c_{m0} as

$$Z_m(\omega) = Z_{m0}(\omega) + mZ_{v0}F(t), \tag{10}$$

where $c_{m0} = \sqrt{\frac{T_0}{\rho_m d}}$ is the sound speed of the unmodulated membrane, $Z_{m0} = Z_m|_{c_m = c_{m0}}$ and $Z_{v0} = c_{m0}\frac{\partial Z_m}{\partial c_m}\Big|_{c_m = c_{m0}}$.

In our previous research [15–18], we have demonstrated that the combination of temporal sinusoidal modulation and a phase difference between the modulation signals constitutes a simple yet typical form of space-time modulation, which can give rise to nonreciprocal acoustic transmission. As one can imagine, this nonreciprocal effect can also be induced by periodic modulation, owing to its underlying mathematical equivalence, as shown in Eq. (1), which can be used to design acoustic isolators. In the following subsections, we will verify the effectiveness and accuracy of the proposed method through the design of two-membrane acoustic isolators under typical periodic space-time modulations, namely square-wave, triangular-wave and sawtooth-wave modulations. It should be noted that the selection of these three types of periodic modulation profiles is based on the considerations of future experimental implementation. In contrast to sinusoidal temporal modulation, the linear variation of parameters with time in these three periodic modulation profiles is more readily achievable and allows for more precise experimental control.

3.1 Square-wave modulation

We begin with the analysis of square-wave modulation. As depicted in Fig. 3(a), the modulation functions $F(t)$ of the two membranes are both standard square waveforms and are identical except for a phase difference ϕ. According to the method outlined above, the square-wave function can be expanded into a Fourier cosine series, given by

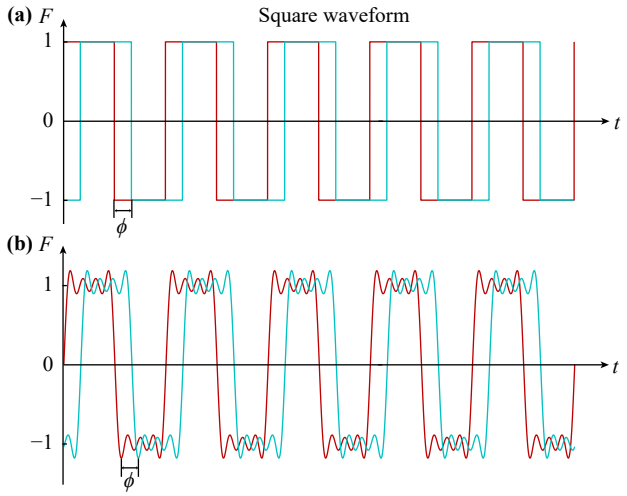

Fig. 3 Square-wave modulation function $F(t)$ applied to the two membranes. **(a)** Ideal waveform used in simulations. **(b)** Harmonic-truncated waveform used in theoretical calculations. Blue line: Membrane 1; Red line: Membrane 2.

$$F(t) = \sum_{N=1}^{\infty} A_N \cos(N\Omega t - \phi_N) \tag{11}$$

The Fourier coefficients A_N and ϕ_N for $F_1(t)$ and $F_2(t)$ are listed in Table 1. In the following theoretical analysis, only the first seven modulation frequency components ($N \leq 7$) are retained, while the higher-order components are neglected. The resulting truncated square waveforms reconstructed from these components are shown in Fig. 3(b).

Without loss of generality, the fundamental modulation frequency is set as $f_m = \Omega/(2\pi) = 200$ Hz for all three modulation types. The design parameter space includes incident wave frequency (also referred to as the operating frequency) and modulation phase difference between two membranes. To evaluate the nonreciprocal performance of the two-membrane system under periodic modulation, two metrics are introduced: the isolation factor $IF = \left|20\log\left(t_0^+/t_0^-\right)\right|$ and transmission asymmetry $TA = \left|t_0^+ - t_0^-\right|$, where t_0^+ and t_0^- denote the transmission coefficients of the fundamental mode in positive and negative directions, respectively.

Figures 4(a) and (b) depict the variation of the isolation factor and transmission asymmetry as functions of the incident wave frequency and modulation phase difference, respectively. A pronounced nonreciprocal band emerges near the resonance frequency for moderate phase differences. The isolation factor can reach up to 23.6 dB, while the maximum transmission asymmetry is approximately 0.7. These results indicate that the two-membrane system under square-wave modulation can achieve strong nonreciprocity with relatively low insertion loss through appropriate selection of modulation parameters. The parameters selected for the simulations are marked by red stars in Figs. 4(a) and (b), corresponding to $f_0 = 2520$ Hz and $\phi = 0.48\pi$, determined based on a trade-off between the isolation factor and transmission asymmetry.

Then we analyze the nonreciprocal (acoustic isolator) behavior of this two-membrane system with the marked optimal modulation parameters. The theoretically calculated transmission coefficients of the generated harmonics in the positive and negative directions are depicted by the black dashed curves in Figs. 4(c) and (d), respectively. A clear nonreciprocal transmission is observed. The fundamental-mode (2520 Hz) transmission coefficients for opposite directions are 0.726 and 0.048, respectively, which correspond to an isolation factor of 23.6 dB and a transmission asymmetry of 0.678. To further demonstrate the nonreciprocal transmission, time-domain simulations are performed using the designed parameters. A monochromatic acoustic wave is incident on the waveguide from one end, and a modulated transmitted signal is obtained at the other end. By applying the Fourier transform, the signal spectrum is obtained, as shown by the red solid curves in Figs. 4(c) and (d). In the positive direction, the transmission coefficient amplitude of the fundamental mode (2520 Hz) is 0.730, while in the negative direction, the transmission coefficient amplitude is only 0.055. The corresponding isolation factor is 23.4 dB, and the transmission asymmetry is 0.675. Note that in the simulations, we adopt the ideal modulation waveform as shown in Fig. 3(a), while in the theoretical calculation the modulation waveform is harmonically truncated and reconstructed as shown in Fig. 3(b). The results from the theoretical calculation and time-domain simulations are in excellent agreement, which effectively validates the theoretical calculation method proposed in this work.

Table 1 Fourier coefficients for square waveforms.

	N	1	2	3	4	5	6	7	...
$F_1(t)$	A_N	$\frac{4}{\pi}$	0	$\frac{4}{3\pi}$	0	$\frac{4}{5\pi}$	0	$\frac{4}{7\pi}$	...
	ϕ_N	$\frac{\pi}{2}+\phi$	0	$\frac{\pi}{2}+3\phi$	0	$\frac{\pi}{2}+5\phi$	0	$\frac{\pi}{2}+7\phi$	...
$F_2(t)$	A_N	$\frac{4}{\pi}$	0	$\frac{4}{3\pi}$	0	$\frac{4}{5\pi}$	0	$\frac{4}{7\pi}$	...
	ϕ_N	$\frac{\pi}{2}$	0	$\frac{\pi}{2}$	0	$\frac{\pi}{2}$	0	$\frac{\pi}{2}$	...

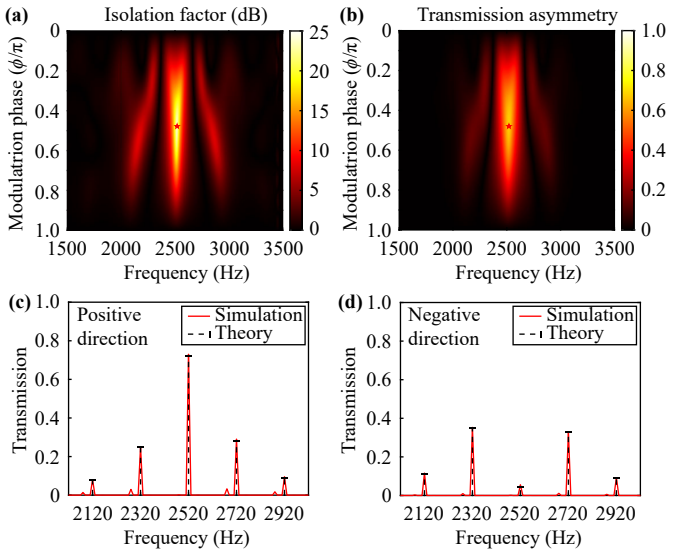

Fig. 4 **(a)** Isolation factor and **(b)** transmission asymmetry of the two-membrane system under square-wave modulation with modulation frequency $f_m = 200$ Hz and modulation depth $m = 0.1 \times \pi/4$. The red star marks the parameters used in the following theoretical and numerical analysis. Transmission of different modes in **(c)** the positive direction and **(d)** the negative direction. Red solid curves: Transmission spectra obtained from time-domain finite element simulations. Black dashed curve: theoretically predicted transmission at the 0^{th}, $\pm1^{\text{st}}$, and $\pm2^{\text{nd}}$ harmonic orders. Higher-order harmonics are negligible and are not shown.

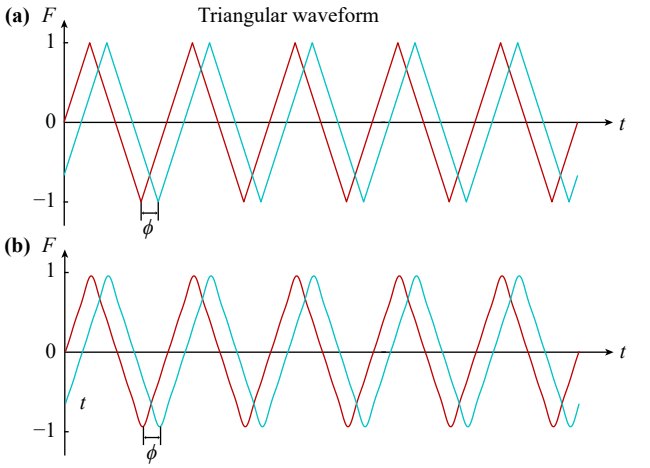

Fig. 5 Triangular-wave modulation functions applied to the two membranes. **(a)** Ideal waveform used in simulations. **(b)** Harmonic-truncated waveform used in theoretical calculations. Blue line: Membrane 1; Red line: Membrane 2.

3.2 Triangular-wave modulation

In this subsection, we follow the same procedure and focus on the analysis of triangular-wave modulation. As depicted in Fig. 5(a), the modulation waveform functions $F(t)$ of the two membranes are both standard triangular waveforms and are identical except for a phase difference ϕ. The Fourier coefficients A_N and ϕ_N for $F_1(t)$ and $F_2(t)$ are listed in Table 2. After truncating the harmonics, the two triangular waveforms reconstructed from these components are shown in Fig. 5(b).

First, we calculate the variation of the isolation factor and transmission asymmetry as functions of the incident wave frequency and modulation phase difference, as shown in Figs. 6(a) and (b), respectively. Compared with the results for square-wave modulation shown in Figs. 4(a) and (b), it can be seen that there are strong similarities between the two modulation schemes.

Then, we choose the optimal incident frequency $f_0 = 2510$ Hz and phase difference $\phi = 0.50\pi$ as marked by red stars in Figs. 6(a) and (b), which are slightly different from those of the square-wave modulation. The theoretically calculated transmission coefficients of the generated harmonics in the positive and negative directions are depicted by the black dashed curves in Figs. 6(c) and (d), respectively. It can be seen that the fundamental-mode (2510 Hz) transmission coefficients for opposite directions are 0.721 and 0.078, respectively, which correspond to an isolation factor of 19.3 dB and a transmission asymmetry of 0.643.

Finally, we conduct the time-domain simulations of triangular-wave modulation with the optimal parameters. The results are depicted by the red solid curves in Figs. 6(c) and (d). In the positive direction, the transmission coefficient amplitude of the fundamental mode (2510 Hz) is 0.725, while in the negative direction, the transmission coefficient amplitude is only 0.084. The corresponding isolation factor is 18.7 dB, and the transmission asymmetry is 0.641. Like the case of square-

Table 2 Fourier coefficients for triangular waveforms.

	N	1	2	3	4	5	6	7	...
$F_1(t)$	A_N	$\frac{8}{\pi^2}$	0	$-\frac{8}{3^2\pi^2}$	0	$\frac{8}{5^2\pi^2}$	0	$-\frac{8}{7^2\pi^2}$	...
	ϕ_N	$\frac{\pi}{2}+\phi$	0	$\frac{\pi}{2}+3\phi$	0	$\frac{\pi}{2}+5\phi$	0	$\frac{\pi}{2}+7\phi$	...
$F_2(t)$	A_N	$\frac{8}{\pi^2}$	0	$-\frac{8}{3^2\pi^2}$	0	$\frac{8}{5^2\pi^2}$	0	$-\frac{8}{7^2\pi^2}$	...
	ϕ_N	$\frac{\pi}{2}$	0	$\frac{\pi}{2}$	0	$\frac{\pi}{2}$	0	$\frac{\pi}{2}$	...

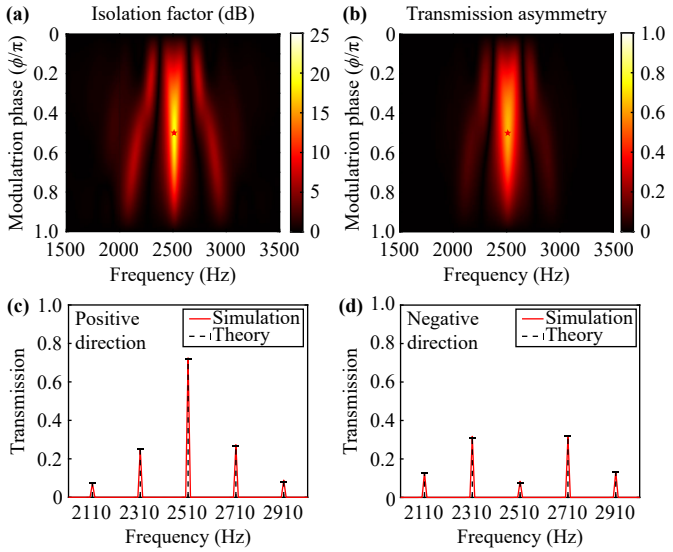

Fig. 6 **(a)** Isolation factor and **(b)** transmission asymmetry of the two-membrane system under triangular-wave modulation with modulation frequency $f_m = 200$ Hz and modulation depth $m = 0.1 \times \pi^2/8$. The red star marks the parameters used in the following theoretical and numerical analysis. Transmission of different modes in **(c)** the positive direction and **(d)** the negative direction. Red solid curves: Transmission spectra obtained from time-domain finite element simulations. Black dashed curves: Theoretically predicted transmission at the 0^{th}, $\pm1^{\text{st}}$, and $\pm2^{\text{nd}}$ harmonic orders. Higher-order harmonics are negligible and not shown.

wave modulation, the results from theoretical calculations and simulations are also in excellent agreement.

3.3 Sawtooth-wave modulation

In this subsection, the analysis of sawtooth-wave modulation is carried out. As depicted in Fig. 7(a), the modulation waveform functions $F(t)$ of the two membranes are both standard sawtooth waveforms and are identical except for a phase difference ϕ. The Fourier coefficients A_N and ϕ_N for $F_1(t)$ and $F_2(t)$ are listed in Table 3. The harmonic-truncated sawtooth waveforms reconstructed from these components are shown in Fig. 7(b).

Firstly, we calculate the variation of the isolation factor and transmission asymmetry as functions of the

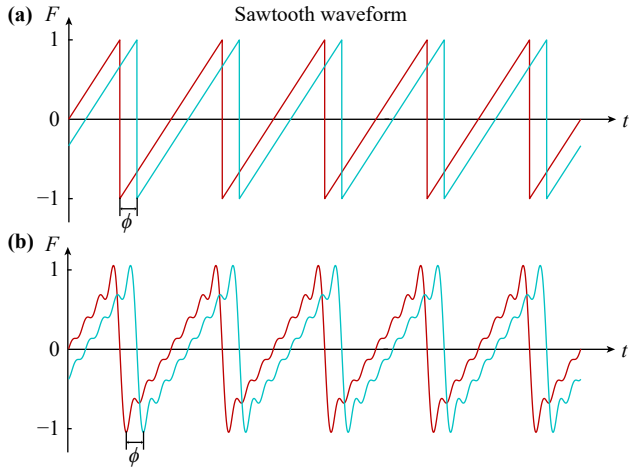

Fig. 7 Sawtooth-wave modulation functions applied to the two membranes. **(a)** Ideal waveform used in simulations. **(b)** Harmonic-truncated waveform used in theoretical calculations. Blue line: Membrane 1; Red line: Membrane 2.

incident wave frequency and modulation phase difference, as shown in Figs. 8(a) and (b) respectively. Compared with the results for square-wave modulation shown in Figs. 4(a) and (b), there are slight differences between the two modulation schemes.

Then, the optimal incident frequency $f_0 = 2560$ Hz and phase difference $\phi = 0.35\pi$ are selected and marked by green stars in Figs. 8(a) and (b), which are clearly different from those of square-wave and triangular-wave modulations. The theoretically calculated transmission coefficients of the generated harmonics in the positive and negative directions are depicted by the black dashed curves in Figs. 8(c) and (d), respectively. It can be seen that the fundamental-mode (2560 Hz) transmission coefficients for opposite directions are 0.634 and 0.135, respectively, corresponding to an isolation factor of 13.4 dB and a transmission asymmetry of 0.499.

Finally, we perform the time-domain simulations for sawtooth-wave modulation using the optimal parameters. The results are shown by the red solid curves in Figs. 8(c) and (d). In the positive direction, the transmission coefficient amplitude of the fundamental mode (2560 Hz) is 0.643, while in the negative direction, it is only 0.130. The corresponding isolation factor is

Table 3 Fourier coefficients for sawtooth waveforms.

	N	1	2	3	4	5	6	7	...
$F_1(t)$	A_N	$\frac{2}{\pi}$	$-\frac{2}{2\pi}$	$\frac{2}{3\pi}$	$-\frac{2}{4\pi}$	$\frac{2}{5\pi}$	$-\frac{2}{6\pi}$	$\frac{2}{7\pi}$	...
	ϕ_N	$\frac{\pi}{2}+\phi$	$\frac{\pi}{2}+2\phi$	$\frac{\pi}{2}+3\phi$	$\frac{\pi}{2}+4\phi$	$\frac{\pi}{2}+5\phi$	$\frac{\pi}{2}+6\phi$	$\frac{\pi}{2}+7\phi$	...
$F_2(t)$	A_N	$\frac{2}{\pi}$	$-\frac{2}{2\pi}$	$\frac{2}{3\pi}$	$-\frac{2}{4\pi}$	$\frac{2}{5\pi}$	$-\frac{2}{6\pi}$	$\frac{2}{7\pi}$	...
	ϕ_N	$\frac{\pi}{2}$	$\frac{\pi}{2}$	$\frac{\pi}{2}$	$\frac{\pi}{2}$	$\frac{\pi}{2}$	$\frac{\pi}{2}$	$\frac{\pi}{2}$	...

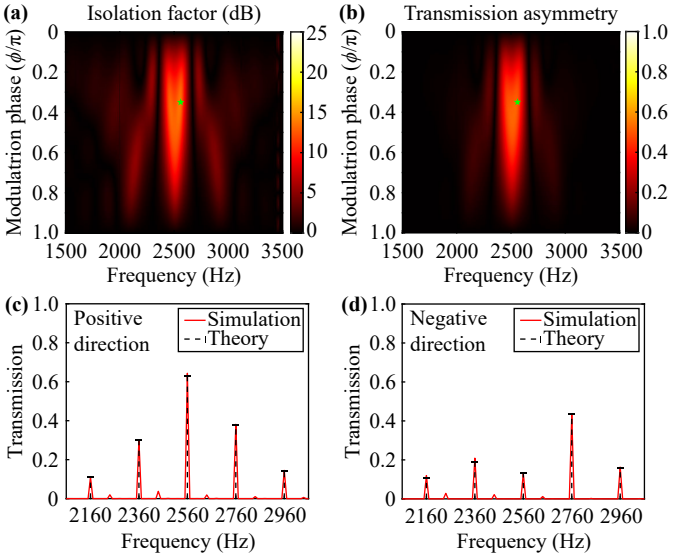

Fig. 8 **(a)** Isolation factor and **(b)** transmission asymmetry of the two-membrane system under sawtooth-wave modulation with modulation frequency $f_m = 200$ Hz and modulation depth $m = 0.1 \times \pi/2$. The green star marks the parameters implemented in the following theoretical and numerical analysis. Transmission of different modes in **(c)** the positive direction and **(d)** the negative direction. Red solid curves: transmission spectra obtained from time-domain finite element simulation. Black dashed curves: theoretically predicted transmission at the 0^{th}, $\pm1^{\text{st}}$, and $\pm2^{\text{nd}}$ harmonic orders. Higher-order harmonics are negligible and not shown.

13.9 dB, and the transmission asymmetry is 0.513. The results from theoretical calculation and time-domain simulation are in excellent agreement.

4 Discussion and conclusion

As the number of matrices has negligible impact on the calculation process of the transfer matrix method, we adopt one of the simplest systems to demonstrate the capabilities of the proposed method in periodic modulation. Results show that the generalized transfer matrix method can help identify the optimal parameters for acoustic isolator design under three typical periodic modulation profiles through parametric sweeps, which is impractical in simulation or experiment. Then, to verify the calculation accuracy, time-domain simulations are performed under the three typical periodic modulations using the optimal parameters. The results from the generalized transfer matrix method and time-domain simulations are in excellent agreement, which effectively validates the proposed method. It should be emphasized that while we present only three representative periodic modulation profiles here, the method is, in fact, applicable to arbitrary periodic modulation profiles. Moreover, it is theoretically extendable to arbitrary temporal modulations, since any modulation profile can be expressed in terms of a Fourier expansion. Although the present work focuses on one-dimensional wave propagation, the framework holds promise for extension to two-dimensional cases. However, such an extension poses challenges, including spatiotemporally coupled modulation of interfacial acoustic impedance, added spatial complexity of the acoustic field distribution, and corresponding increase in computational demands.

Apart from theoretical calculation method itself, we also find meaningful insights in the study of periodic modulation in this work. Figures of isolation factor and transmission asymmetry for the three different periodic modulations show that the overall nonreciprocal acoustic transmission effect under sawtooth-wave modulation is significantly weaker than those under square-wave and triangular-wave modulations. This result can be explained by the Fourier expansion of the modulation waveform. In theory, periodic modulation can be regarded as multi-frequency sinusoidal modulation, in which the fundamental modulation frequency plays the dominant role, while higher-order frequencies have diminishing influence. In square-wave and triangular-wave modulations, the second-order modulation frequency component is zero. In contrast, in the sawtooth-wave modulation, the proportion of the second-order modulation frequency component reaches half of the fundamental, which likely diminishes the modulation effect. Moreover, to support this conjecture, the modulation depth in all three modulation profiles was carefully designed to ensure that the fundamental modulation coefficient equals 0.1, identical to that used in sinusoidal modulation in our previous work [18]. A comparison of the positive and negative transmission coefficients under four modulation profiles shows that square-wave and triangular-wave modulations yield results nearly identical to sinusoidal modulation, whereas sawtooth-wave modulation leads to a marked reduction in the positive transmission coefficient and a pronounced increase in the negative coefficient, providing additional evidence for our hypothesis.

The primary focus of this work is the development and validation of the generalized transfer matrix method, demonstrated via a simple two-membrane system for a basic nonreciprocal acoustic effect. Nevertheless, this approach establishes a foundation for a wide range of potential design possibilities. On the one hand, multiple modulation profiles including square, triangular, and sawtooth waveforms, have the potential to generate diverse and novel functionalities. On the other hand, since periodic modulation is inherently a multi-frequency sinusoidal modulation, it is possible to go beyond the limitations of traditional periodic modulation profiles and directly design the parameters of each modulation frequency components, thereby greatly enhancing design flexibility and opportunities. Moreover,

as the design freedom expands, artificial intelligence techniques can be integrated to facilitate the exploration of a broad spectrum of potential nonreciprocal effects.

To conclude, a generalized transfer matrix method for one-dimensional periodic space-time modulated system is proposed and demonstrated. This method overcomes the limitations associated with sinusoidal modulation profiles in space-time modulated metamaterials, making the design of space-time modulated meta-devices more practical and applicable. It should be noted, however, that the proposed model of a one-dimensional space-time modulated system is idealized, as it does not account for damping and nonlinear effects, which may lead to discrepancies between theoretical predictions and experimental results, particularly in systems with high damping or strong modulation. We anticipate that this generalized transfer matrix method will serve as a valuable technique and fundamental framework for various studies in space-time modulated metamaterials. Future research will focus on addressing the effects of neglected loss while further exploring the potential directions mentioned above.

Declarations The authors have no conflicts to disclose.

Data availability The data that support the findings of this study are available from the corresponding author upon reasonable request.

Acknowledgements This research was supported by Zhejiang Provincial Natural Science Foundation of China under Grant No. LQ24E050016, Huzhou Science and Technology Project (Grant No. 2022YZ14), and the Scientific Research Fund of Zhejiang Provincial Education Department (Grant No. Y202351044). X.Z. also wishes to thank the great help of Junfei Li from Purdue University.

References

1. N. A. Estep, D. L. Sounas, J. Soric, and A. Alù, Magnetic-free non-reciprocity and isolation based on parametrically modulated coupled-resonator loops, *Nat. Phys.* 10(12), 923 (2014)
2. Y. Hadad, D. L. Sounas, and A. Alù, Space-time gradient metasurfaces, *Phys. Rev. B* 92(10), 100304 (2015)
3. F. Ruesink, M. A. Miri, A. Alù, and E. Verhagen, Nonreciprocity and magnetic-free isolation based on optomechanical interactions, *Nat. Commun.* 7(1), 13662 (2016)
4. M. A. Miri, F. Ruesink, E. Verhagen, and A. Alù, Optical nonreciprocity based on optomechanical coupling, *Phys. Rev. Appl.* 7(6), 064014 (2017)
5. A. Y. Song, Y. Shi, Q. Lin, and S. Fan, Direction-dependent parity-time phase transition and nonreciprocal amplification with dynamic gain-loss modulation, *Phys. Rev. A* 99(1), 013824 (2019)
6. S. Taravati and G. V. Eleftheriades, Space-time medium functions as a perfect antenna-mixer-amplifier transceiver, *Phys. Rev. Appl.* 14(5), 054017 (2020)
7. P. A. Huidobro, M. G. Silveirinha, E. Galiffi, and J. Pendry, Homogenization theory of space-time metamaterials, *Phys. Rev. Appl.* 16(1), 014044 (2021)
8. S. Taravati and G. V. Eleftheriades, Microwave space-time-modulated metasurfaces, *ACS Photonics* 9(2), 305 (2022)
9. Q. Hu, K. Chen, Y. Zheng, Z. Xu, J. Zhao, J. Wang, and Y. Feng, Broadband wireless communication with space-time-varying polarization-converting metasurface, *Nanophotonics* 12(7), 1327 (2023)
10. Y. Liu, Y. Wang, X. Fu, L. Shi, F. Yang, J. Luo, Q. Y. Zhou, Y. Fu, Q. Chen, J. Y. Dai, L. Zhang, Q. Cheng, and T. J. Cui, Toward sub-terahertz: Space-time coding metasurface transmitter for wideband wireless communications, *Adv. Sci. (Weinh.)* 10(29), 2304278 (2023)
11. R. Fleury, D. L. Sounas, C. F. Sieck, M. R. Haberman, and A. Alù, Sound isolation and giant linear nonreciprocity in a compact acoustic circulator, *Science* 343(6170), 516 (2014)
12. R. Fleury, D. L. Sounas, and A. Alù, Subwavelength ultrasonic circulator based on spatiotemporal modulation, *Phys. Rev. B* 91(17), 174306 (2015)
13. R. Fleury, A. B. Khanikaev, and A. Alù, Floquet topological insulators for sound, *Nat. Commun.* 7(1), 11744 (2016)
14. J. Li, C. Shen, X. Zhu, Y. Xie, and S. A. Cummer, Nonreciprocal sound propagation in space-time modulated media, *Phys. Rev. B* 99(14), 144311 (2019)
15. J. Li, X. Zhu, C. Shen, X. Peng, and S. A. Cummer, Transfer matrix method for the analysis of space-time-modulated media and systems, *Phys. Rev. B* 100(14), 144311 (2019)
16. C. Shen, J. Li, Z. Jia, Y. Xie, and S. A. Cummer, Nonreciprocal acoustic transmission in cascaded resonators via spatiotemporal modulation, *Phys. Rev. B* 99(13), 134306 (2019)
17. C. Shen, X. Zhu, J. Li, and S. A. Cummer, Nonreciprocal acoustic transmission in space-time modulated coupled resonators, *Phys. Rev. B* 100(5), 054302 (2019)
18. X. Zhu, J. Li, C. Shen, X. Peng, A. Song, L. Li, and S. A. Cummer, Non-reciprocal acoustic transmission via space-time modulated membranes, *Appl. Phys. Lett.* 116(3), 034101 (2020)
19. X. Zhu, J. Li, C. Shen, G. Zhang, S. A. Cummer, and L. Li, Tunable unidirectional compact acoustic amplifier via space-time modulated membranes, *Phys. Rev. B* 102(2), 024309 (2020)
20. Z. Chen, Y. Peng, H. Li, J. Liu, Y. Ding, B. Liang, X. Zhu, Y. Lu, J. Cheng, and A. Alù, Efficient nonreciprocal mode transitions in spatiotemporally modulated acoustic metamaterials, *Sci. Adv.* 7(45), eabj1198 (2021)
21. M. H. Fakheri, H. Rajabalipanah, and A. Abdolali, Spatiotemporal binary acoustic metasurfaces, *Phys. Rev. Appl.* 16(2), 024062 (2021)
22. J. Kang and M. R. Haberman, Sound diffusion with spatiotemporally modulated acoustic metasurfaces, *Appl. Phys. Lett.* 121(18), 181703 (2022)
23. X. Wen, X. Zhu, A. Fan, W. Y. Tam, J. Zhu, H. W. Wu, F. Lemoult, M. Fink, and J. Li, Unidirectional amplification with acoustic non-hermitian space-time varying metamaterial, *Commun. Phys.* 5(1), 18 (2022)

24. K. Pham and A. Maurel, How space-time modulations modify spoof surface plasmons and scattering properties in acoustic metagratings, *Phys. Rev. B* 108(2), 024303 (2023)
25. X. Zhu and C. Shen, An acoustic metamaterial with space-time modulated density, *J. Acoust. Soc. Am.* 156(6), 3984 (2024)
26. G. Trainiti and M. Ruzzene, Non-reciprocal elastic wave propagation in spatiotemporal periodic structures, *New J. Phys.* 18(8), 083047 (2016)
27. Y. Wang, B. Yousefzadeh, H. Chen, H. Nassar, G. Huang, and C. Daraio, Observation of nonreciprocal wave propagation in a dynamic phononic lattice, *Phys. Rev. Lett.* 121(19), 194301 (2018)
28. B. M. Goldsberry, S. P. Wallen, and M. R. Haberman, Nonreciprocity and mode conversion in a spatiotemporally modulated elastic wave circulator, *Phys. Rev. Appl.* 17(3), 034050 (2022)
29. S. T. Brothelande, C. Cröenne, F. Allein, J. O. Vasseur, M. Amberg, F. Giraud, and B. Dubus, Experimental evidence of nonreciprocal propagation in space-time modulated piezoelectric phononic crystals, *Appl. Phys. Lett.* 123(20), 201701 (2023)
30. H. Moussa, G. Xu, S. Yin, E. Galiffi, Y. Ra'di, and A. Alù, Observation of temporal reflection and broadband frequency translation at photonic time interfaces, *Nat. Phys.* 19(6), 863 (2023)
31. T. R. Jones, A. V. Kildishev, M. Segev, and D. Peroulis, Time-reflection of microwaves by a fast optically-controlled time-boundary, *Nat. Commun.* 15(1), 6786 (2024)
32. L. Bar-Hillel, A. Dikopoltsev, A. Kam, Y. Sharabi, O. Segal, E. Lustig, and M. Segev, Time refraction and time reflection above critical angle for total internal reflection, *Phys. Rev. Lett.* 132(26), 263802 (2024)
33. C. Ellouzi, F. Aghdasi, A. Zabihi, S. Zhao, and C. Shen, Phase-engineered 3D-printed metalenses for spatial and spectral control of underwater acoustic vortex beams, *Front. Phys. (Beijing)* 21(8), 085201 (2026)
34. Z. Hao, H. Chen, Y. Yin, C. W. Qiu, S. Zhu, and H. Chen, Efficient conversion of acoustic vortex using extremely anisotropic metasurface, *Front. Phys. (Beijing)* 19(4), 42202 (2024)
35. M. Mostafa, M. Mirmoosa, E. Galiffi, S. Yin, A. Alù, and S. Tretyakov, Broadband amplification of light through adiabatic spatiotemporal modulation, arXiv: 2506.20358 (2025)
36. E. Lustig, O. Segal, S. Saha, C. Fruhling, V. M. Shalaev, A. Boltasseva, and M. Segev, Photonic time-crystals - fundamental concepts, *Opt. Express* 31(6), 9165 (2023)
37. Z. Liu, X. Zhu, Z. G. Zhang, W. M. Zhang, X. Chen, Y. Q. Yang, R. W. Peng, M. Wang, J. Li, and H. W. Wu, Direct observation of k-gaps in dynamically modulated phononic time crystal, arXiv: 2505.07160 (2025)
38. Z. Liu, K. Yi, H. Sun, R. Zhu, X. Zhou, G. Hu, and G. Huang, Inherent temporal metamaterials with unique time-varying stiffness and damping, *Adv. Sci. (Weinh.)* 11(43), 2404695 (2024)
39. P. K. Tien and H. Suhl, A traveling-wave ferromagnetic amplifier, *Proceedings of the IRE* 46(4), 700 (1958)
40. P. K. Tien, Parametric amplification and frequency mixing in propagating circuits, *J. Appl. Phys.* 29(9), 1347 (1958)
41. H. Nassar, H. Chen, A. N. Norris, M. R. Haberman, and G. Huang, Non-reciprocal wave propagation in modulated elastic metamaterials, *Proc. Royal Soc. Math. Phys. Eng. Sci.* 473(2202), 20170188 (2017)
42. H. Moussa, G. Xu, S. Yin, E. Galiffi, Y. Ra'di, and A. Alù, Observation of temporal reflection and broadband frequency translation at photonic time interfaces, *Nat. Phys.* 19(6), 863 (2023)